Relationships between piezoelectric and energy-harvesting characteristics of 1–2–2 composites based on domain-engineered single crystals

V. Yu. Topolov,[a] A. N. Isaeva,[a] C. R. Bowen,[b] and B. O. Protsenko[a]

[a]Department of Physics, Southern Federal University, 344090 Rostov-on-Don, Russia

[b]Department of Mechanical Engineering, University of Bath, BA2 7AY Bath, UK

Abstract. The paper reports on the piezoelectric performance, electromechanical coupling and related energy-harvesting figures of merit of three forms of 1–2–2 composites based on domain-engineered single crystals. The effect of the single-crystal piezoelectric properties and elastic properties of the laminar polymer matrix on the appropriate figures of merit of the composite is studied. The main active components of the studied composites are [001]-poled perovskite-type single crystals with chemical compositions: $0.92Pb(Zn_{1/3}Nb_{2/3})O_3 - 0.08PbTiO_3$, $0.67Pb(Mg_{1/3}Nb_{2/3})O_3 - 0.33PbTiO_3$ and $[Li_x(K_{1-y}Na_y)_{1-x}](Nb_{1-z}Ta_z)O_3$:Mn, where $x = 0.06$, $y = 0.1–0.3$, $z = 0.07–0.17$, and the level of Mn doping is 0.25 mol. %. Examples of non-monotonic volume-fraction dependences of the piezoelectric properties, figures of merit and anisotropy factors are analysed. New diagrams are first built to demonstrate the volume-fraction regions where a large anisotropy of the piezoelectric coefficients d_{3j}^* and electromechanical coupling factors k_{3j}^* is achieved, and where energy-harvesting figures of merit of the composite are at least five times larger than analogous parameters of single-crystal components. The studied 1–2–2 composites are of interest as anisotropic materials with high piezoelectric sensitivity and large figures of merit which are important for sensor, energy-harvesting and related applications.

Keywords Piezo-active composite; Piezoelectric properties; Electromechanical coupling factor; Figure of merit; Anisotropy factors

PACS 77.65.-j: Piezoelectricity and electromechanical effects; 77.84.Lf: Composite materials; and 77.84.-s: Dielectric; piezoelectric; ferroelectric; and antiferroelectric materials

Running head: **Relationships between characteristics of 1–2–2s**

Contact V. Yu. Topolov vutopolov@sfedu.ru

1. Introduction

Since the 2000s, there has been significant interest in piezo-active composites that are based on domain-engineered single crystals (SCs) [1–4] and described by 1–3 connectivity in terms of the pioneering work of Newnham et al. [5]. Due to their outstanding electromechanical properties, poled domain-engineered relaxor-ferroelectric $(1 - x)Pb(Mg_{1/3}Nb_{2/3})O_3 - xPbTiO_3$ (PMN–*x*PT) [6] and $(1 - x)Pb(Zn_{1/3}Nb_{2/3})O_3 - xPbTiO_3$ (PZN–*x*PT) [7, 8] SCs with a perovskite-type structure and compositions chosen near the morphotropic phase boundary [9] are often used as the primary piezoelectric components of 1–3 [2–4] and related [10, 11] composites. Based on publications in the 2010–20s, one can state the piezoelectric performance and related parameters of lead-free domain-engineered SCs [12, 13], and related composite structures [14] are of specific interest since they play a key role in manufacturing environmentally friendly piezotechnical and energy-harvesting devices by replacing lead-containing ferroelectric ceramics, such as $Pb(Zr, Ti)O_3$ [15]. Chemical compositions of the high-performance ferroelectric lead-free SCs are chosen among the alkali niobates – alkali tantalates [12, 13] with a perovskite-type structure. An important example of a modification of the 1–3 composite structure is a 1–2–2 SC / Polymer I / Polymer II composite [4, 16] that exhibits a high piezoelectric sensitivity, strong electromechanical coupling, and large hydrostatic parameters. To date, no comparison of the performance of the 1–2–2 composites has been carried out in detail because of the complex dependence of their effective electromechanical properties on a system of parameters [4]; these include volume fractions of components, shape of the SC rod base, and so on. Moreover, the influence of an anisotropy of piezoelectric properties on the hydrostatic, energy-harvesting and other parameters of the 1–2–2 composites is of an independent interest to optimise performance for specific applications. The aim of the present paper is to compare the performance of three types of 1–2–2 SC-based composites and to show the links between their piezoelectric properties and energy-harvesting figures of merit (FOMs), especially where there is a large piezoelectric anisotropy. The large piezoelectric anisotropy and related features of

electromechanical coupling are important [10, 14] in the context of piezotechnical applications where the longitudinal oscillation mode plays an important role.

In the composites to be analysed in the present paper, the SC component is either lead-containing (such as PMN–*x*PT or PZN–*x*PT) or lead-free, but in each case the SC component is domain-engineered and poled along the specific crystallographic direction. Hence, it is also important to compare parameters of the lead-free 1–2–2 composite to those of the lead-containing composites with the same connectivity pattern.

2. Model of the composite, its effective properties and related parameters

The 1–2–2 composite consists of a system of long ferroelectric SC rods surrounded by a laminar matrix, as shown in Fig. 1, that contains two kinds of polymers termed ‘Polymer I’ and ‘Polymer II’. The domain-engineered SC rods are poled along [001] of the perovskite unit cell (see inset 1 in Fig. 1), and are characterised by a spontaneous polarisation $\boldsymbol{P}_s^{(1)} \uparrow\uparrow OX_3$ and arranged in a regular square in the (X_1OX_2) plane. The crystallographic axes $X^{(1)}$, $Y^{(1)}$ and $Z^{(1)}$ of each SC rod obey conditions $X^{(1)} \parallel OX_1$, $Y^{(1)} \parallel OX_2$ and $Z^{(1)} \parallel OX_3$. Hereafter we consider two shapes of the SC rod, namely, a parallelepiped with a square base, and a cylinder. Cross sections of these SC rods by the (X_1OX_2) plane are shown in insets 2 and 3 of Fig. 1. The matrix that surrounds the SC rods is laminar (see inset 4 in Fig. 1), and is characterised by 2–2 connectivity (in terms of work [5]) and by the regular arrangement of the polymer layers with interfaces oriented parallel to the (X_1OX_2) plane. The OX_3 axis is regarded as a poling axis of the composite sample as a whole, see Fig. 1.

The effective electromechanical (i.e., elastic, piezoelectric and dielectric) properties of the 1–2–2 composite are evaluated in two stages as follows. In the first stage the effective properties of the laminar Polymer I / Polymer II matrix are determined using the matrix method [4, 10, 11] that is suitable to predict the properties of the 2–2 and 1–3 composites with planar microgeometry. The second stage involves an averaging procedure to find the full set of

electromechanical constants of the 1–2–2 composite by means of either the matrix method [10, 11, 16] (for the composite with the parallelepiped-shaped SC rods) or the effective field method [10, 11] (for the composite with the cylindrical SC rods). In both the aforementioned methods, the electromechanical interaction between the aligned piezoelectric SC rods and the shape of their lateral surfaces are taken into account [10, 11]. As a result of the averaging procedure, the effective electromechanical properties of the 1–2–2 composite are represented in the matrix form, namely,

$$|| F_{MM}^{*} || = \begin{pmatrix} || s^{*E} || & || d^{*} ||^{t} \\ || d^{*} || & || \varepsilon^{*\sigma} || \end{pmatrix} \tag{1}$$

by using the matrix method in the second stage, and

$$|| F_{EFM}^{*} || = \begin{pmatrix} ||c^{*E}|| & || e^{*} ||^{t} \\ ||e^{*}|| & -||\varepsilon^{*\xi}|| \end{pmatrix} \tag{2}$$

by using the effective field method in the second stage. In Eq. (1) $|| s^{*E} ||$ is a 6 × 6 matrix of elastic compliances measured at E = const, $|| d^{*} ||$ is a 6 × 3 matrix of piezoelectric coefficients, $|| \varepsilon^{*\sigma} ||$ is a 3 × 3 matrix of dielectric permittivities measured at mechanical stress σ = const, and the superscript t means the transposition of the matrix. In Eq. (2) $|| c^{*E} ||$ is a 6 × 6 matrix of elastic moduli at E = const, $|| e^{*} ||$ is a 6 × 3 matrix of piezoelectric coefficients, and $|| \varepsilon^{*\xi} ||$ is a 3 × 3 matrix of dielectric permittivities at mechanical strain ξ = const. Elements of the $|| F_{MM}^{*} ||$ and $|| F_{EFM}^{*} ||$ matrices from Eqs. (1) and (2) depend on the volume fraction of the SC component m in the composite and on the volume fraction of Polymer I m_s in the matrix, see Fig. 1. The effective electromechanical properties from Eqs. (1) and (2) are considered as properties homogenised in the long-wave approximation [10, 11]. This approximation means that a wavelength of an external field is much longer than a thickness of any polymer layer in the composite sample shown in Fig. 1. It should be added that interrelations between the full sets of electromechanical constants from Eqs. (1) and (2) are described in terms of formulae [17] for a piezoelectric medium.

In our study we analyse the following effective parameters of the 1–2–2 composite:

(i) piezoelectric coefficients d_{3j}^{*} and g_{3j}^{*},

(ii) electromechanical coupling factors (ECFs)

$$k_{3j}^{*} = d_{3j}^{*} / (\varepsilon_{33}^{*\sigma} s_{jj}^{*E})^{1/2}, \quad (3)$$

(iii) traditional (squared) energy-harvesting FOMs

$$(Q_{3j}^{*})^2 = d_{3j}^{*} g_{3j}^{*}, \quad (4)$$

(iv) modified FOMs [18, 19] introduced for a stress-driven system

$$F_{3j}^{*\sigma} = L_{3j}^{*} (Q_{3j}^{*})^2, \quad (5)$$

and

(v) anisotropy factors

$$\zeta_d^{*} = d_{33}^{*} / d_{31}^{*} \text{ and } \zeta_k^{*} = k_{33}^{*} / k_{31}^{*} = \zeta_d^{*} (s_{11}^{*E} / s_{33}^{*E})^{1/2}. \quad (6)$$

The piezoelectric coefficients d_{3j}^{*} and g_{3j}^{*} from Eq. (4) are related in accordance with the formula [17]

$$d_{3j}^{*} = \varepsilon_{3f}^{*\sigma} g_{fj}^{*}. \quad (7)$$

In Eq. (5)

$$L_{3j}^{*} = [(k_{3j}^{*})^{-1} - ((k_{3j}^{*})^{-2} - 1)^{1/2}]^2 / (k_{3j}^{*})^2 \quad (8)$$

is the ‘maximum output electrical energy / stored electrical energy’ ratio [18] that depends on ECFs k_{3j}^{*} from Eq. (3), where j = 1 or 2 (transverse piezoelectric effect), and j = 3 (longitudinal piezoelectric effect). In Eq. (8) the ECFs k_{3j}^{*} are taken as absolute values in accordance with work [18, 19]. Along with ECFs k_{3j}^{*} from Eq. (3), FOMs $(Q_{3j}^{*})^2$ and $F_{3j}^{*\sigma}$ from Eqs. (4) and (5), respectively, are of importance to evaluate the effectiveness of a piezoelectric material from a viewpoint of energy conversion. Knowledge of the anisotropy factors ζ_d^{*} and ζ_k^{*} from Eqs. (6) is important to determine conditions when a transverse oscillation mode of the composite sample (Fig. 1) is negligible in comparison to the longitudinal oscillation mode excited along the poling axis OX_3.

3. Components of 1–2–2 composites

To evaluate the effective electromechanical properties and related parameters of the 1–2–2 composites, we use experimental data (Tables 1 and 2) on the properties of SC and polymer components. Among the domain-engineered SCs of particular interest, we have chosen PZN–0.08PT and PMN–0.33PT due to their large piezoelectric charge coefficients d_{3j} (see data in Table 1), and lead-free KNNTL-Mn with large piezoelectric voltage coefficients g_{3j} (see data in Table 3). The three aforementioned SCs are considered as poled along [001] of the perovskite unit cell. The chemical composition of the KNNTL-Mn SC is $[Li_x(K_{1-y}Na_y)_{1-x}](Nb_{1-z}Ta_z)O_3$:Mn, where x = 0.06, y = 0.1–0.3, z = 0.07–0.17, and the level of Mn doping is 0.25 mol. % [13]. Irrespective of the composition, the SCs from Tables 1 and 3 are characterised by a small anisotropy of piezoelectric coefficients $d_{33} / | d_{31} | = g_{33} / | g_{31} | \approx 2$ and by a considerable elastic anisotropy.

Despite differences between the electromechanical constants of the SCs (see Table 1), their longitudinal ECFs k_{33} differ to a small degree, and values of $k_{33} \approx 0.93$–0.97 (see Table 3) are large as compared to k_{33} of many perovskite-type ferroelectric ceramics [10]. The longitudinal FOM $(Q_{33})^2$ of the SC depends on its piezoelectric coefficient d_{33} due to the relation,

$$(Q_{33}^*)^2 = (d_{33}^*)^2 / \varepsilon_{33}^{*\sigma} \qquad (9)$$

that holds in accordance with Eqs. (4) and (7). It should be mentioned that at the volume fraction m = 1, equalities $d_{33}^* = d_{33}$ and $(Q_{33}^*)^2 = (Q_{33})^2$ hold. Taking into account Eqs. (6), (7) and (9), we note that the piezoelectric anisotropy factor ζ_d^* is also involved in the following relations:

$\zeta_d^* = g_{33}^* / g_{31}^*$ and $(\zeta_d^*)^2 = (Q_{33}^*)^2 / (Q_{31}^*)^2$.

In contrast to the SC components from Tables 1 and 2, araldite and polyethylene (PE) from Table 2 are piezo-passive [20, 21]. We note the appreciable difference between elastic compliances s_{ab} of araldite and PE. Hereafter the volume fraction m_s refers to the polymer component with the smaller absolute values of compliances $| s_{ab} |$, namely, the araldite (see Table

2). This means that increasing the volume fraction m_s in the composite matrix will lead to a decrease in its longitudinal elastic compliance $s_{33}^{(m)}$.

4. Effective parameters of 1–2–2 composites

4.1. Volume-fraction dependences

Important results on the effective parameters evaluated by means of the matrix method described in Section 2 are shown in Figs. 2 and 3. These results are related to the 1–2–2 composites that contain parallelepiped-shaped SC rods with square bases, see insets 1 and 2 in Fig. 1. By analogy with traditional 1–3 ferroelectric ceramic / polymer composites [10, 11], the piezoelectric coefficients d_{3j}^* and ECFs k_{3j}^* exhibit a monotonic behaviour on increasing the volume fraction m, and we do not show such examples in the present paper.

Of interest are non-monotonic volume-fraction (m) dependences of the piezoelectric coefficients g_{3j}^* and FOMs $(Q_{33}^*)^2$ and $F_{33}^{*\sigma}$, see curves 1, 2, 3, and 5 in Fig. 2. The graphs in Fig. 2 suggest that a large anisotropy of the piezoelectric coefficients g_{3j}^* and FOMs $(Q_{3j}^*)^2$ and $F_{3j}^{*\sigma}$ is achieved at specific volume-fraction ranges, irrespective of the SC component. The non-monotonic behaviour of g_{3j}^* of curves 1 and 2 in Fig. 2 is due to the effective combination of the piezoelectric and dielectric properties in the 1–3-type composite [11]. Hereby, the extremum points of the piezoelectric coefficient

$$g_{33}^* = d_{33}^* / \varepsilon_{33}^{*\sigma} \tag{10}$$

at $m << 1$ are accounted for by the monotonic decrease in d_{33}^* (relatively rapid increase) and $\varepsilon_{33}^{*\sigma}$ (relatively slow increase). A similar combination of properties leads to a non-monotonic behaviour of FOMs $(Q_{33}^*)^2$ from Eq. (9) and $F_{33}^{*\sigma} \sim (Q_{33}^*)^2$ in accordance with Eq. (5). It should be noted that all the maximum points of the effective parameters shown in Fig. 2 are related to volume fractions of SC in the range of $0.005 < m < 0.09$. Such small volume fractions of SC ($m < 0.03$) can give rise to technological challenges on manufacturing, and to avoid such problems, one can choose a volume fraction of SC $m = 0.1$ or larger, at which a high level of the effective

parameters (e.g. $g_{33}^{*} \sim 1$ V·m / N or $F_{33}^{*\sigma} \sim 10^{-10}$ Pa^{-1}) is achieved. Some important examples of the performance of the 1–2–2 composites at m = 0.1 and 0.2 are shown in Fig. 3. It should be added that the large anisotropy of FOMs $F_{3j}^{*\sigma}$ is observed in the wide m range (see Fig. 2), irrespective of the SC component. Such a performance is related to the active role of the laminar polymer matrix, whose elastic anisotropy influences the piezoelectric properties and related FOMs of the composite.

As seen from Fig. 3, the volume-fraction range of $0.2 \le m_s \le 0.5$ is of interest for the following reasons:

(i) the longitudinal piezoelectric coefficients d_{33}^{*} and g_{33}^{*}, and ECF k_{33}^{*} undergo a decrease to a restricted degree, as seen in curves 1–3 of Fig. 3, and

(ii) conditions for a large anisotropy

$$| \zeta_d^{*} | \ge 5 \text{ and } | \zeta_k^{*} | \ge 5 \qquad (11)$$

hold simultaneously (see curves 4 and 5 in Fig. 3). The presence of $\min\zeta_d^{*}$ at $m_s \approx 0.30$–0.35 irrespective of the SC component in the composite (see curves 4 in Fig. 3) is mainly due to the large elastic anisotropy of the 2–2 araldite / PE matrix [16]. Moreover, the relatively small volume fraction of SC m = 0.1 or 0.2 means that the 2–2 matrix plays an important role in forming a large piezoelectric anisotropy of the 1–2–2 composite. We remind the reader that a small anisotropy of d_{3j} is typical of the SC components, see Table 1, and therefore, cannot favour the validity of conditions (11) with an active influence of the polymer matrix. A simple comparison of Fig. 3, a with Fig. 3, d shows that an increase in the volume fraction of SC from m = 0.1 to m = 0.2 leads to less favoured conditions for validity of inequalities (11). For instance, we see that at m = 0.2, the inequality $| \zeta_k^{*} | < 5$ holds in a specific m_s range, see curve 5 in Fig. 3, d. Taking into account the relation (6) between the anisotropy factors ζ_k^{*} and ζ_d^{*}, we again emphasise the important role of the elastic anisotropy of the polymer matrix that influences the $s_{11}^{*E} / s_{33}^{*E}$ ratio from Eqs. (6).

4.2. New diagrams of volume-fraction regions of interest

To show volume-fraction regions where conditions (11) for a large anisotropy are valid, we have built three new diagrams in Fig. 4. At these diagrams one can see areas 1 and 2, which are related to conditions (11), and areas 3 and 4 which are concerned with large longitudinal FOMs of the studied composites. Conditions for large FOMs are given by

$$(Q_{33}^{*})^2 / (Q_{33}^{(1)})^2 \geq 5 \quad (12)$$

and

$$F_{33}^{*\sigma} / F_{33}^{(1),\sigma} \geq 5. \quad (13)$$

FOMs $(Q_{33}^{(1)})^2$ and $F_{33}^{(1),\sigma}$ from conditions (12) and (13), respectively, refer to the SC component, and values of these FOMs are given in Table 3. It is worth noting that the studied composites differ owing to validity of conditions (11)–(13) in the aforementioned volume-fraction range of $0.2 \leq m_s \leq 0.5$, see Fig. 4.

For the PZN–0.08PT-based composite, conditions (11) are valid as shown in Fig. 4, a. The PMN–0.33PT-based composite exhibits a validity of conditions (11) and (12) in Fig. 4, b, however area 3 of validity of condition (12) is relatively small. The KNNTL-Mn-based composite is of particular interest due to validity of the full set of conditions (11)–(13), see Fig. 4, c. In our opinion, a validity of conditions (11)–(13) is due to the small elastic compliances $| s_{ab}^{(1),E} |$ of the KNNTL-Mn SC among the SC components from Table 1. This leads to the largest difference between the elastic properties of the SC rod and laminar polymer matrix, which exhibits the appreciable elastic anisotropy [16].

As follows from the diagrams shown in Fig. 4, the volume-fraction (m) range to be considered for potential applications is [0.05, 0.2]. This corresponds to a composite architecture where the volume fraction of the laminar polymer matrix is large, and due to its elastic anisotropy, this matrix has a strong influence on the piezoelectric properties, ECFs and FOMs of the 1–2–2 composite.

5. Comparison of parameters

The volume-fraction dependences and diagrams in Figs. 2–4 have been evaluated by means of the matrix method (see Section 2), and the 1–2–2 composites considered in Section 4 contain parallelepiped-shaped SC rods; see inset 2 in Fig. 1. In the case of a system of cylindrical SC rods in a composite (see inset 3 in Fig. 1), we apply the effective field method in the second stage of averaging, as described in Section 2. Table 4 shows data on the piezoelectric properties, ECFs and FOMs which have been evaluated for the PZN–0.08PT-based composites. Good agreement is observed between parameters related to the longitudinal response of the composites, irrespective of the cross section of their SC rods (see insets 2 and 3 in Fig. 1). Moreover, our evaluation by means of the effective field method suggests that conditions (11) hold and conditions (12) and (13) are invalid for the PZN–0.08PT-based composite with cylindrical SC rods.

A range of effective parameters of PMN–0.33PT-based composites with a similar microgeometry are compared in work [4]; see Table S3 in Electronic Supplementary Information. These parameters are evaluated by means of the matrix method and finite element method, and agreement between data is observed at various volume fractions m and m_s.

The studied 1–2–2 composites have advantages over known piezo-active 1–3 composites and textured ferroelectric ceramics due to the large FOMs $(Q_{33}^*)^2 \sim 10^{-10}$ Pa^{-1} and $F_{33}^{*\sigma} \sim 10^{-10}$ Pa^{-1}, ECF $k_{33}^* \approx 0.8$–0.9, and anisotropy factors $|\zeta_d^*|$ and $|\zeta_k^*|$ which obey conditions (11). For comparison we mention a 1–3 lead-free composite based on $0.965(K_{0.45}Na_{0.55})(Nb_{0.96}Sb_{0.04})O_3$–$0.0375Bi_{0.5}Na_{0.5}Zr_{0.85}Hf_{0.15}O_3$ ceramic: according to experimental results [22], the piezoelectric coefficient d_{33}^* of this 1–3 composite equals 350 pC / N. A 1–3 PZT-7A ceramic / araldite composite from work [23] is characterised by $L_{33}^* \approx 0.29$, $(Q_{33}^*)^2 \approx 16 \cdot 10^{-12}$ Pa^{-1} and $F_{33}^{*\sigma} \approx 4.6 \cdot 10^{-12}$ Pa^{-1} at a volume fraction of ferroelectric ceramic $m_{cer} = 0.2$. For a 1–3 composite based on the [001]-poled domain-engineered PMN–0.30PT SC [2], experimental results at $m = 0.56$ lead to $L_{33}^* \approx 0.39$, $(Q_{33}^*)^2 \approx 100 \cdot 10^{-12}$ Pa^{-1} and $F_{33}^{*\sigma} \approx 39 \cdot 10^{-12}$ Pa^{-1}. A textured relaxor-ferroelectric $Pb(Mg_{1/3}Nb_{2/3})O_3 – PbZrO_3 – PbTiO_3$ ceramic in the poled state is characterised by

the largest $(Q_{33})^2$ value that equals $59.18 \cdot 10^{-12}$ Pa^{-1} [24]. Clearly the lead-free composites examined here have potential provide improved FOMs compared to their lead-based counterparts.

6. Conclusions

The present paper has been devoted to the study on the set of effective parameters of piezo-active 1–2–2 SC / Polymer I / Polymer II composites. The main component of these composites is the domain-engineered [001]-poled perovskite-type SC, as outlined in Table 1. The SC is either lead-containing (PMN–0.33PT or PZN–0.08PT) or lead-free (KNNTL-Mn). The SCs from Tables 1 and 3 are characterised by either a very large piezoelectric charge coefficient d_{33} (i.e., high piezoelectric activity of PMN–0.33PT or PZN–0.08PT) or a very large piezoelectric voltage coefficient g_{33} (i.e., high piezoelectric sensitivity of KNNTL-Mn). The influence of the piezoelectric properties and anisotropic Polymer I / Polymer II matrix on the performance of the studied 1–2–2 composites has been analysed. On taking into account the large effective piezoelectric coefficients, ECFs, FOMs, and anisotropy factors of the studied composites (see Figs. 2–4 and Table 4), we pay special attention to following volume-fraction ranges: $0.05 \le m \le 0.2$ (the SC component in the presence of the laminar matrix with the large volume fraction) and $0.2 \le m_s \le 0.5$. The composite based on the KNNTL-Mn SC obeys conditions (11)–(13) in specific m and m_s ranges (see Fig. 4, c). The performance of the remaining composites makes it possible to state validity of conditions (11) only (see Fig. 4, a related to the PZN–0.08PT-based composite) or validity of conditions (11) and (12) (see Fig. 4, b related to the PMN–0.33PT-based composite). In Table 4 we observe good agreement between the parameters associated with the longitudinal response of the composites that contain SC rods with a specific geometry. The studied 1–2–2 composites can be used as active elements of piezoelectric sensors, transducers and energy-harvesting devices where the longitudinal piezoelectric effect and related ECF and FOMs play the leading role.

Declaration of Competing Interest

The authors declare that they have no known competing financial interests or personal relationships that could have appeared to influence the work reported in this paper.

Acknowledgements

The authors would like to thank Prof. Dr. A. E. Panich and Prof. Dr. I. A. Parinov (Southern Federal University, Russia), and Prof. Dr. P. Bisegna (University of Rome Tor Vergata, Italy) for their interest in the performance of modern piezoelectric materials. This study was supported by the Russian Foundation for Basic Research (project No. 20-38-90163).

References

1. K. Ren, Y. Liu, X. Geng, H. F. Hofmann, and Q. M. Zhang, Single crystal PMN–PT/epoxy 1–3 composite for energy-harvesting application. *IEEE Trans. Ultrason., Ferroelec., a. Freq. Contr*. **53**, 631 (2006).
2. F. Wang, C. He, Y. Tang, X. Zhao, and H. Luo, Single crystal $0.7Pb(Mg_{1/3}Nb_{2/3})O_3$–$0.3PbTiO_3$ / epoxy 1–3 piezoelectric composites prepared by the lamination technique. *Mater. Chem. Phys*. **105**, 273 (2007).
3. D. Zhou, K. H. Lam, Y. Chen, Q. Zhang, Y. C. Chiu, H. Luo, J. Dai, and H. L. W. Chan, Lead-free piezoelectric single crystal based 1–3 composites for ultrasonic transducer applications. *Sens. Actuators A – Phys.* **182**, 95 (2012).
4. C. R. Bowen, V. Yu. Topolov, A. N. Isaeva, and P. Bisegna, Advanced composites based on relaxor-ferroelectric single crystals: from electromechanical coupling to energy-harvesting applications. *CrystEngComm* **18**, 5986 (2006).
5. R. E. Newnham, D. P. Skinner, and L. E. Cross, Connectivity and piezoelectric-pyroelectric composites. *Mater. Res. Bull*. **13**, 525 (1978).
6. R. Zhang, B. Jiang, and W. Cao, Elastic, piezoelectric, and dielectric properties of multidomain $0.67Pb(Mg_{1/3}Nb_{2/3})O_3$–$0.33PbTiO_3$ single crystals. *J. Appl. Phys*. **90**, 3471 (2001).
7. J. Yin, B. Jiang, and W. Cao, Elastic, piezoelectric, and dielectric properties of $0.955Pb(Zn_{1/3}Nb_{2/3})O_3$–$0.045PbTiO_3$ single crystals. *IEEE Trans. Ultrason., Ferroelec., a. Freq. Contr*. **47**, 285 (2000).
8. R. Zhang, B. Jiang, W. Cao, and A. Amin, Complete set of material constants of $0.93Pb(Zn_{1/3}Nb_{2/3})O_3$–$0.07PbTiO_3$ domain engineered single crystal. *J. Mater. Sci. Lett.* **21**, 1877 (2002).
9. B. Noheda, Structure and high-piezoelectricity in lead oxide solid solutions. *Curr. Opin. Solid State Mater. Sci*. **6**, 27 (2002).

10. C. R. Bowen, V. Yu. Topolov, and H. A. Kim, *Modern Piezoelectric Energy-Harvesting Materials.* Springer International Publishing, Cham, 2016.

11. V. Yu. Topolov, C. R. Bowen, and P. Bisegna, *Piezo-Active Composites. Microgeometry – Sensitivity Relations*. Springer International Publishing, Cham, 2018.

12. L. M. Zheng, X. Q. Huo, R. Wang, J. J. Wang, W. H. Jiang, and W. W. Cao, Large size lead-free (Na, K)(Nb, Ta)O_3 piezoelectric single crystal: growth and full tensor properties. *CrystEngComm* **15**, 7718 (2013).

13. X. Huo, R. Zhang, L. Zheng, S. Zhang, R. Wang, J. Wang, S. Sang, B. Yang, and W. Cao, (K, Na, Li)(Nb, Ta)O_3:Mn lead-free single crystal with high piezoelectric properties. *J. Am. Cer. Soc*. **98**, 1829 (2015).

14. V. Yu. Topolov, A. N. Isaeva, and P. Bisegna, Novel lead-free composites with two porosity levels: large piezoelectric anisotropy and high sensitivity. *J. Phys. D: Appl. Phys.* **53**, 395303 (2020).

15. E. K. Akdogan, M. Allahverdi, and A. Safari, Piezoelectric composites for sensor and actuator applications. *IEEE Trans. Ultrason., Ferroelec., a. Freq. Contr*. **52**, 746 (2005).

16. V. Yu. Topolov, C.R. Bowen, A. N. Isaeva, and A.A. Panich, Theoretical study on the piezoelectric performance of lead-free 1–3-type composites. Phys. Stat. Solidi A **215**, 1700548 (2018).

17. T. Ikeda, *Fundamentals of Piezoelectricity*. Oxford University Press, Oxford, New York, Toronto, 1990.

18. J. I. Roscow, H. Pearce, H. Khanbareh, S. Kar-Narayan, and C.R. Bowen, Modified energy harvesting figures of merit for stress- and strain-driven piezoelectric systems. *Eur. Phys. J. Special Topics* **228**, 1537 (2019).

19. D. B. Deutz, J.-A. Pascoe, B. Schelen, S. van der Zwaag, D. M. de Leeuw, and P. Groen, Analysis and experimental validation of the figure of merit for piezoelectric energy harvesters. *Mater. Horiz*. **5**, 444 (2018).

20. F. Levassort, M. Lethiecq, C. Millar, and L. Pourcelot, Modeling of highly loaded 0–3 piezoelectric composites using a matrix method. *IEEE Trans. Ultrason., Ferroelec., a. Freq. Contr*. **45**, 1497 (1998).

21. K. E. Evans and K. L. Alderson, The static and dynamic moduli of auxetic microporous polyethylene. *J. Mater. Sci. Lett*. **11**, 1721 (1992).

22. Q. Ke, W. H. Liew, H. Tao, J. Wu, and K. Yao, KNNS-BNZH Lead-free 1–3 piezoelectric composite for ultrasonic and photoacoustic imaging. *IEEE Trans. Ultrason., Ferroelec., a. Freq. Contr*. **66**, 1395 (2019).

23. H. L. W. Chan and J. Unsworth, Simple model for piezoelectric ceramic/polymer 1–3 composites used in ultrasonic transducer applications. *IEEE Trans. Ultrason., Ferroelec., a. Freq. Contr*. **36**, 434 (1989).

24. Y. Yan, K.-H. Cho, D. Maurya, A. Kumar, S. Kalinin, A. Khachaturyan, and S. Priya, Giant energy density in [001]-textured $Pb(Mg_{1/3}Nb_{2/3})O_3 - PbZrO_3 - PbTiO_3$ piezoelectric ceramics. *Appl. Phys. Lett*. **102**, 042903 (2013).

Table 1. Experimental room-temperature elastic compliances s_{ab}^{E} (in 10^{-12} Pa^{-1}), piezoelectric coefficients d_{ij} (in pC / N), and dielectric permittivity $\varepsilon_{pp}^{\sigma}$ of [001]-poled domain-engineered SCs[a]

SCs	s_{11}^{E}	s_{12}^{E}	s_{13}^{E}	s_{33}^{E}	s_{44}^{E}	s_{66}^{E}	d_{31}	d_{33}	d_{15}	$\varepsilon_{11}^{\sigma}/\varepsilon_0$	$\varepsilon_{33}^{\sigma}/\varepsilon_0$
PZN–0.08PT [8]	87.0	–13.1	–70.0	141	15.8	15.4	–1455	2890	158	2900	7700
PMN–0.33PT [6]	69.0	–11.1	–55.7	119.6	14.5	15.2	–1330	2820	146	1600	8200
KNNTL-Mn [13]	33.4	–7.36	–25.8	57.7	12.8	13.5	–260	545	66	400	650

[a]Data are related to the main crystallographic axes of the SC. Macroscopic symmetry of the [001]-poled domain-engineered SCs is 4*mm* [4, 6, 8, 13].

Table 2. Experimental room-temperature elastic compliances s_{ab} (in 10^{-12} Pa^{-1}) and dielectric permittivity ε_{pp} of piezo-passive polymers

Polymers	s_{11}	s_{12}	$\varepsilon_{pp}/\varepsilon_0$
Araldite [11, 20]	216	–78	4.0
Polyethylene (high-density) [11, 21]	1540	–517	2.3

Table 3. Piezoelectric coefficients g_{3j} (in mV·m / N), electromechanical coupling factors k_{3j}, and FOMs $(Q_{3j})^2$ (in 10^{-12} Pa^{-1}), and F_{3j}^{σ} (in 10^{-12} Pa^{-1}) of [001]-poled domain-engineered SCs listed in Table 1

SCs	g_{33}	g_{31}	k_{33}	k_{31}	$(Q_{33})^2$	$(Q_{31})^2$	F_{33}^{σ}	F_{31}^{σ}
PZN–0.08PT	42.4	–21.4	0.932	–0.598	123	31.1	66.1	9.57
PMN–0.33PT	39.8	–18.8	0.969	–0.602	112	25.0	72.3	7.72
KNNTL-Mn	94.7	–45.2	0.946	–0.593	51.6	11.8	29.4	3.61

Table 4. Effective parameters calculated for two modifications of the 1–2–2 PZN–0.08PT SC / araldite / polyethylene (PE) composite

m_s	m	Composite with the parallelepiped-shaped SC rods					Composite with the cylindrical SC rods				
		d_{33}^*, pC/N	g_{33}^*, mV·m/N	$(Q_{33}^*)^2$, 10^{-12} Pa^{-1}	k_{33}^*	$F_{33}^*\sigma$, 10^{-12} Pa^{-1}	d_{33}^*, pC/N	g_{33}^*, mV·m/N	$(Q_{33}^*)^2$, 10^{-12} Pa^{-1}	k_{33}^*	$F_{33}^*\sigma$, 10^{-12} Pa^{-1}
0.25	0.05	810	625	506	0.800	198	821	628	515	0.802	202
	0.10	1290	363	468	0.862	207	1300	364	475	0.863	210
	0.20	1850	197	364	0.899	176	1850	197	364	0.899	177
	0.50	2510	83.2	209	0.923	109	2510	83.2	209	0.923	109
0.30	0.05	776	615	477	0.793	184	787	618	486	0.795	188
	0.10	1250	360	450	0.859	196	1260	361	455	0.860	200
	0.20	1800	196	354	0.897	170	1810	197	356	0.897	171
	0.50	2490	83.1	207	0.922	108	2490	83.1	207	0.922	108
0.35	0.05	742	605	449	0.786	171	752	608	457	0.789	175
	0.10	1210	357	430	0.854	186	1220	358	436	0.856	189
	0.20	1760	195	344	0.895	164	1770	196	346	0.895	166
	0.50	2460	82.9	204	0.922	106	2470	83.0	204	0.922	106

Figure captions to the paper

"Relationships between piezoelectric and energy-harvesting characteristics of 1–2–2 composites based on domain-engineered single crystals"

by V. Yu. Topolov et al.

Fig. 1. Schematic of the 1–2–2 SC – polymer I / polymer II composite. ($X_1X_2X_3$) is a rectangular co-ordinate system, m and 1 – m are volume fractions of the SC rods and surrounding laminar matrix, respectively. m_s is the volume fraction of Polymer I in the matrix with 2–2 connectivity.

Fig. 2. Non-monotonic volume-fraction (m) dependences of piezoelectric coefficients g_{3j}^* and FOMs $(Q_{3j}^*)^2$ and $F_{3j}^{*\sigma}$ of 1–2–2 composites at m_s = 0.30: a, PZN–0.08PT SC / araldite / PE and b, KNNTL-Mn SC / araldite / PE.

Fig. 3. Volume-fraction (m_s) dependences of longitudinal piezoelectric coefficients d_{33}^* and g_{33}^*, ECF k_{33}^*, and anisotropy factors ζ_d^* and ζ_k^* of 1–2–2 composites at the volume fraction of SC m = const: a, PZN–0.08PT SC / araldite / PE (m = 0.1), b, PMN–0.33PT SC / araldite / PE (m = 0.1), c, KNNTL-Mn SC / araldite / PE (m = 0.1), and d, PZN–0.08PT SC / araldite / PE (m = 0.2).

Fig. 4. Diagrams that show volume-fraction (m, m_s) regions where conditions for the large anisotropy of piezoelectric coefficients d_{3j}^* and k_{3j}^* hold, and large longitudinal FOMs $(Q_{33}^*)^2$ and $F_{33}^{*\sigma}$ of 1–2–2 composites are achieved: a, PZN–0.08PT SC / araldite / PE, b, PMN–0.33PT SC / araldite / PE, and c, KNNTL-Mn SC / araldite / PE.

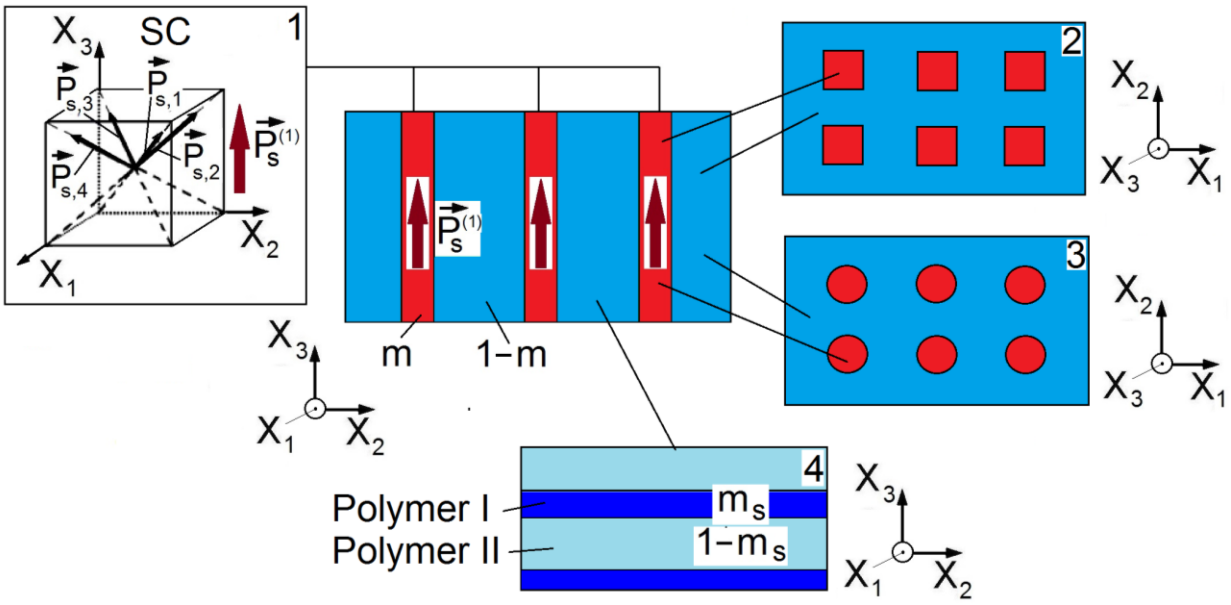

Fig. 1

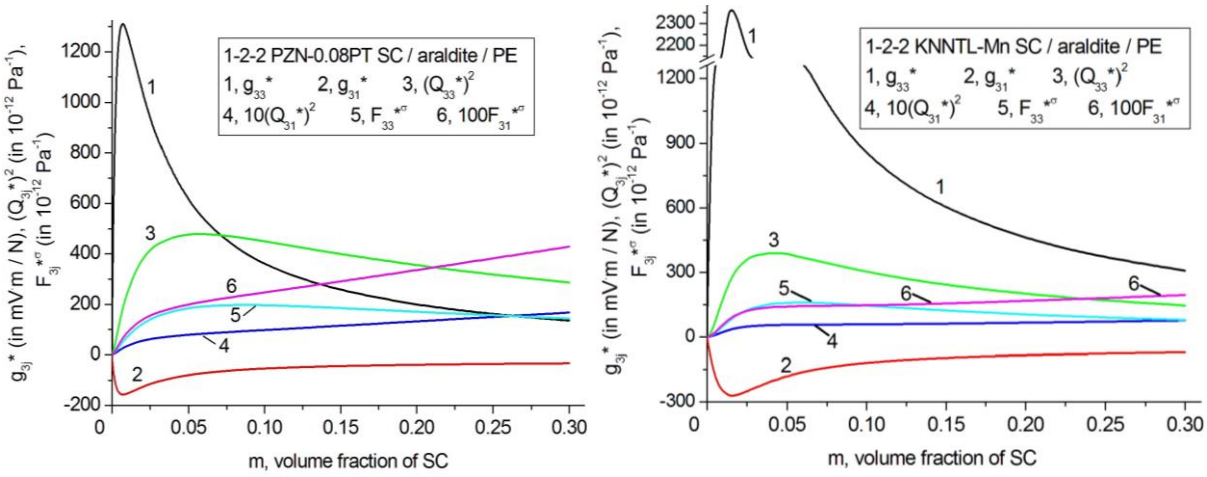
1-2-2 PZN-0.08PT SC / araldite / PE
1, g33* 2, g31* 3, (Q33*)2
4, 10(Q31*)2 5, F33*σ 6, 100F31*σ
g3j* (in mVm / N), (Q3j*)2 (in 10-12 Pa-1),
F3j*σ (in 10-12 Pa-1)
m, volume fraction of SC
1-2-2 KNNTL-Mn SC / araldite / PE
1, g33* 2, g31* 3, (Q33*)2
4, 10(Q31*)2 5, F33*σ 6, 100F31*σ
g3j* (in mVm / N), (Q3j*)2 (in 10-12 Pa-1),
F3j*σ (in 10-12 Pa-1)
m, volume fraction of SC

a b

Fig. 2

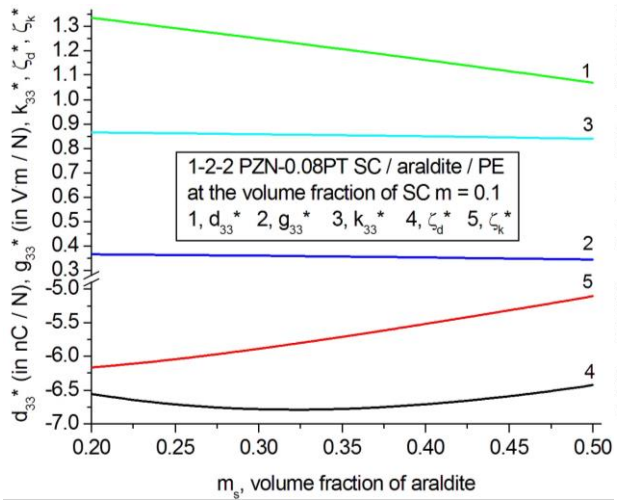
1-2-2 PZN-0.08PT SC / araldite / PE
at the volume fraction of SC m = 0.1
1, d33* 2, g33* 3, k33* 4, ζd* 5, ζk*
d33* (in nC / N), g33* (in V m / N), k33*, ζd*, ζk*
ms, volume fraction of araldite

a

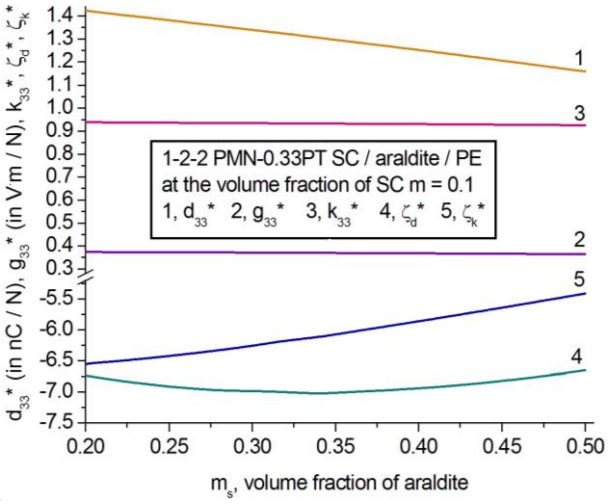
1-2-2 PMN-0.33PT SC / araldite / PE
at the volume fraction of SC m = 0.1
1, d33* 2, g33* 3, k33* 4, ζd* 5, ζk*
d33* (in nC / N), g33* (in V m / N), k33*, ζd*, ζk*
ms, volume fraction of araldite

b

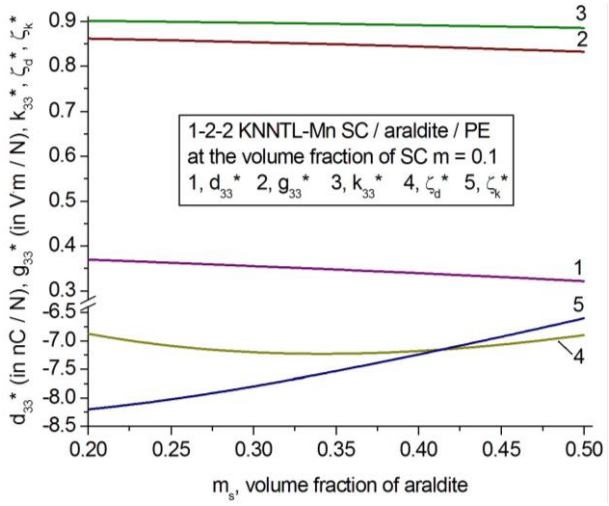
1-2-2 KNNTL-Mn SC / araldite / PE
at the volume fraction of SC m = 0.1
1, d33* 2, g33* 3, k33* 4, ζd* 5, ζk*
d33* (in nC / N), g33* (in V m / N), k33*, ζd*, ζk*
ms, volume fraction of araldite

c

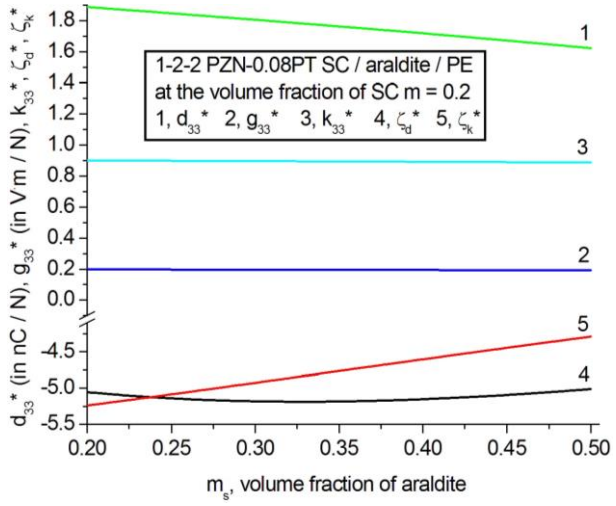
1-2-2 PZN-0.08PT SC / araldite / PE
at the volume fraction of SC m = 0.2
1, d33* 2, g33* 3, k33* 4, ζd* 5, ζk*
d33* (in nC / N), g33* (in V m / N), k33*, ζd*, ζk*
ms, volume fraction of araldite

d

Fig. 3

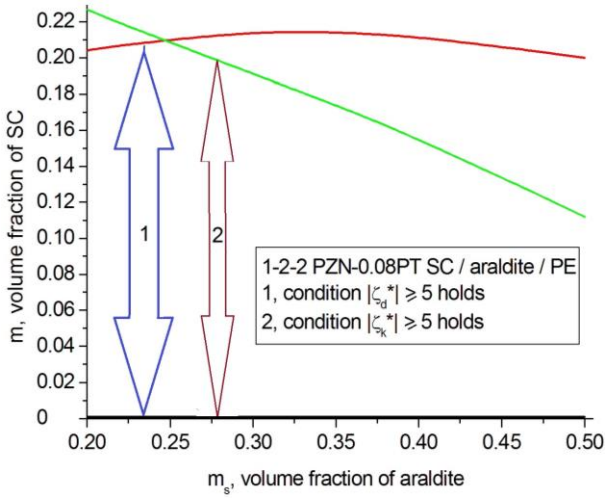
m, volume fraction of SC
m_s, volume fraction of araldite
1-2-2 PZN-0.08PT SC / araldite / PE
1, condition |ζ_d*| ⩾ 5 holds
2, condition |ζ_k*| ⩾ 5 holds
1
2

a

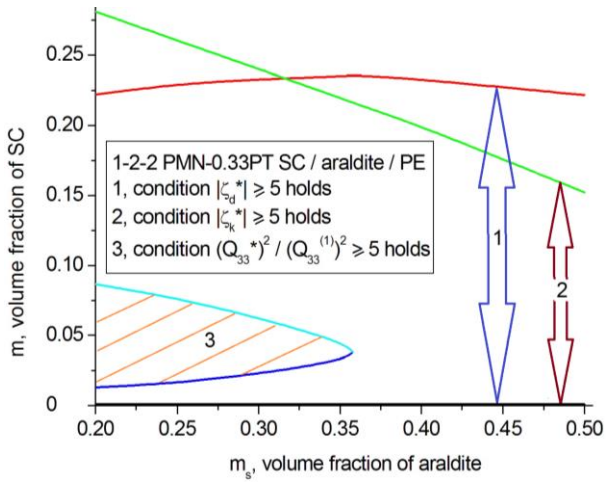
m, volume fraction of SC
m_s, volume fraction of araldite
1-2-2 PMN-0.33PT SC / araldite / PE
1, condition |ζ_d*| ⩾ 5 holds
2, condition |ζ_k*| ⩾ 5 holds
3, condition (Q_33*)^2 / (Q_33^(1))^2 ⩾ 5 holds
1
2
3

b

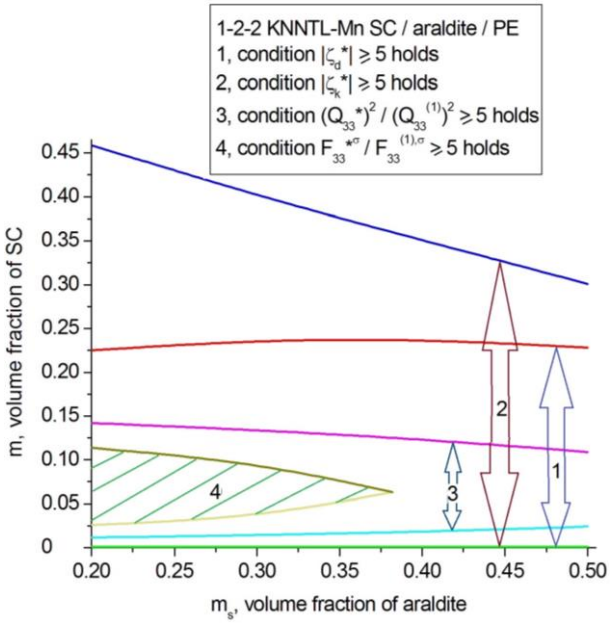
m, volume fraction of SC
m_s, volume fraction of araldite
1-2-2 KNNTL-Mn SC / araldite / PE
1, condition |ζ_d*| ⩾ 5 holds
2, condition |ζ_k*| ⩾ 5 holds
3, condition (Q_33*)^2 / (Q_33^(1))^2 ⩾ 5 holds
4, condition F_33^*σ / F_33^(1),σ ⩾ 5 holds
1
2
3
4

c

Fig. 4